

Efficient light upconversion via resonant exciton-exciton annihilation of dark excitons in few-layer transition metal dichalcogenides

Yi-Hsun Chen^{1,2,†}, Ping-Yuan Lo^{3†}, Kyle W. Boschen^{2,4}, Guan-Hao Peng³, Chun-Jui Huang³, Luke N. Holtzman⁵, Chih-En Hsu⁶, Yung-Ning Hsu⁶, Madisen Holbrook⁷, Wei-Hua Wang⁸, Katayun Barmak⁵, James Hone⁹, Pawel Hawrylak¹⁰, Hung-Chung Hsueh⁶, Jeffrey A. Davis^{2,4}, Shun-Jen Cheng^{3,*}, Michael S. Fuhrer^{1,2,11}, Shao-Yu Chen^{2,12,13,*}*

¹ School of Physics and Astronomy, Monash University, Clayton, Victoria 3800, Australia

² Australian Research Council Centre of Excellence in Future Low-Energy Electronics Technologies (FLEET), Monash University, Clayton, Victoria 3800, Australia

³ Department of Electrophysics, National Yang Ming Chiao Tung University, Hsinchu 300 093, Taiwan.

⁴ Optical Sciences Centre, Swinburne University of Technology, Hawthorn, VIC 3122, Australia.

⁵ Department of Applied Physics and Applied Mathematics, Columbia University, New York, New York 10027, United States

⁶ Department of Physics, Tamkang University, New Taipei City, 251301 Taiwan

⁷ Department of Physics, Columbia University, New York NY 10027, USA

⁸ Institute of Atomic and Molecular Sciences, Academia Sinica, Taipei 10617, Taiwan

⁹ Department of Mechanical Engineering, Columbia University, New York, New York 10027, United States

¹⁰ Department of Physics, University of Ottawa, Ottawa, Ontario, K1N 6N5, Canada

¹¹ Monash Centre for Atomically Thin Materials, Monash University, Clayton, 3800, VIC, Australia

¹² Center for Condensed Matter Sciences, National Taiwan University, Taipei 10617, Taiwan

¹³ Center of Atomic Initiative for New Material, National Taiwan University, Taipei 10617, Taiwan

† Equally contributed

Keywords: light upconversion, exciton-exciton annihilation, dark excitons, transition metal dichalcogenides, 2D materials

ABSTRACT

Materials capable of light upconversion—transforming low-energy photons into higher-energy ones—are pivotal in advancing optoelectronics, energy solutions, and photocatalysis. However, the discovery in various materials pays little attention on few-layer transition metal dichalcogenides, primarily due to their indirect bandgaps and weaker light-matter interactions. Here, we report a pronounced light upconversion in few-layer transition metal dichalcogenides through upconversion photoluminescence spectroscopy. Our joint theory-experiment study attributes the upconversion photoluminescence to a resonant exciton-exciton annihilation involving a pair of dark excitons with opposite momenta, followed by the spontaneous emission of upconverted bright excitons, which can have a high upconversion efficiency. Additionally, the upconversion photoluminescence is generic in MoS₂, MoSe₂, WS₂, and WSe₂, showing a high tuneability from green to ultraviolet light (2.34–3.1 eV). The findings pave the way for further exploration of light upconversion regarding fundamental properties and device applications in two-dimensional semiconductors.

INTRODUCTION

Upconversion photoluminescence (UPL) is an anti-Stokes phenomenon of light-matter interactions in which a material radiatively emits photons at an energy higher than the excitation energy. Since the process is able to generate high-energy photons, UPL is of interest in a wide range of applications across various fields such as biology¹⁻³, medicine^{4,5}, and energy⁶⁻⁸. Starting from the very first rare-earth doped nanomaterials⁹, the demonstration of UPL has been reported in inorganic^{10,11}, organic^{12,13}, and organic-inorganic hybrid^{14,15} semiconductors. Recent advancements, particularly in molecular systems employing triplet-triplet annihilation, have achieved high-quantum efficiency and/or low excitation density in the upconversion process.^{16,17} However, there is still a growing demand for solid-state alternatives due to their enhanced durability and compatibility with existing semiconductor manufacturing technologies, which could open doors for broader applications.

Exciton-exciton annihilation (EEA) has a fundamental advantage over other upconversion mechanisms for spontaneous light upconversion in solid-state materials. EEA is a two-body process in which one exciton transfers its energy and momentum to another, effectively doubling the energy of the resulting exciton.¹⁸ The rate of EEA exhibits a quadratic dependence on exciton density¹⁹, which is more efficient than the cubic dependence in three-body processes, such as Auger recombination²⁰, especially in the low-density regime. Despite its potential, EEA phenomena require a dominance of excitonic effects in materials, a condition challenging to achieve in bulk semiconductors due to their small exciton binding energies. Atomically thin 2D semiconducting materials, on the other hand, possess excitons with binding energies reaching several hundreds of meV because of the reduced dielectric screening.²¹ Moreover, they host a rich exciton landscape from the intriguing electronic band structures within the Brillouin zone, making them ideal candidates for exploring EEA-driven light upconversion. Indeed, EEA has been demonstrated in low-dimensional materials such as carbon nanotubes^{19,22}, graphene nanoribbons²³, quantum wells²⁴, quantum dots²⁵, and even 2D semiconductors²⁶⁻²⁸. However, the UPL under the EEA principle has rarely been reported.

In this work, we report light upconversion in few-layer transition metal dichalcogenides (TMDs) via a resonant EEA of dark excitons. The resonant EEA involves two momentum-indirect dark excitons with opposite momenta upconverting to higher-energy zero-momentum excitons at Γ valley, supported by layer-dependent dark/bright exciton energies observed in both experiments and theoretical calculations. The quadratic power dependence is characterised in WSe₂ atomic layers by using power dependent measurements, indicating EEA as the mechanism for the upconversion process. We also show that the UPL, initiated by using the continuous-wave laser with a fairly low-power density, is fundamentally different from second harmonic generation (SHG), which often necessitates high-power

density through a pulsed laser. Lastly, our study showcases that UPL is remarkably tuneable through material choice (WSe₂, WS₂, MoS₂, and MoSe₂) and layer number, with upconversion photon energy ranging from 2.34 to 3.1 eV. Such tunability underscores the strong layer-dependent energy of dark excitons, originating from significant interlayer Coulomb interactions and quantum confinement effects inherent in atomically thin TMDs.

RESULTS AND DISCUSSION

The initial investigation focuses on identifying excitonic species and UPL in few-layer WSe₂. The fabrication of WSe₂ samples is described in Methods. The thickness of the samples is identified using optical contrast and low-wavenumber Raman spectroscopy (see Extended Data Fig. 1). Figures 1a,b compare the absorbance and UPL spectra, respectively, of a 5L WSe₂ sample at 80 K. The absorbance spectrum (Figure 1a) reveals four pronounced peaks attributed to bright excitons, which are labelled according to their electron/hole configurations, denoted as MN_{*i*}, where M and N represent the momentum of the electron and hole in the hexagonal Brillouin zone, respectively, and *i* indicates the index in ascending energy order for identical configurations. The corresponding electron/hole configurations are schematically illustrated in Figure 1c. From low to high energy, the first and second peaks, labelled KK_A and KK_B, correspond to the traditionally known A and B excitons respectively. At higher energy, we assigned the peaks to QQ and ΓΓ excitons based on our theoretical analysis of excitonic band structures (further details in **Supplementary note 1**) and the prior experiments²⁹. Notably, ΓΓ excitons are composed of electrons with negative effective mass and holes with positive effective mass. Such atypical conduction and valence bands may result in a nesting of excitonic bands with a high joint density of states.^{30–32}

In the UPL spectroscopy, we collect luminescence signals spanning energies both below and above the excitation energy (2.33 eV), yielding a typical PL (upconversion PL) spectrum represented by the blue (ruby) curves in Figure 1b. Sharp features adjacent to 2.33 eV are attributed to Raman scattering by WSe₂. The PL emission from KK_A and KK_B excitons becomes exceedingly weak in 5L WSe₂ due to its indirect bandgap. Meanwhile, KK_A emission is overwhelmed by the PL signals from Al₂O₃ substrate noted in grey shadow (see Extended Data Fig. 2 for PL spectrum of 5L WSe₂ on a SiO₂/Si substrate). Below the KK_A emission, we detect a faint PL peak from the lowest-energy momentum-indirect (dark) excitons, labelled as X_D, at approximately 1.31 eV, which is attributed to QK or QΓ excitons.^{33,34} In the upconversion PL spectrum, we observe a notable emission of UPL around 2.64 eV, which is approximately twice the energy of the X_D peak. Intriguing, the UPL intensity is significantly higher than the X_D in the typical PL spectrum, suggesting an efficient light upconversion

process. A detailed examination of the UPL emission (see the inset in Fig. 1b) reveals that the line profile can be modelled with two peaks: one at higher energy (coloured in orange) well-described by a Gaussian function and the other at lower energy (coloured in light green) described by a Lorentzian. The Gaussian peak primarily contributes to the UPL and is strongly correlated to X_D , which will be analysed in Figure 2; hence, we named it as upconverted excitons (X_{up}). On the other hand, the Lorentzian is located close to but not directly at the $\Gamma\Gamma$ exciton energy seen in the absorbance spectrum. To be clear, we named it as high-lying excitons (HX) instead of $\Gamma\Gamma$ excitons. We note that the Lorentzian profile of HX suggests an ultrafast recombination lifetime³⁵, consistent with the PL emission from high-lying excitons with a large binding energy of up to 0.6–0.7 eV³⁶.

The correlation between dark excitons and UPL is further examined with layer-dependent UPL measurements. Figure 2a presents X_D emissions of 2–6 L WSe₂, exhibiting a red shift in emission energy from 1.553 (2L) to 1.294 eV (6L), consistent with the evolution of the electronic band structure as the layer thickness increases.³⁷ Figure 2b shows the corresponding UPL spectra fitted with two components, HX and X_{up} , as mentioned in the inset of Figure 1b. The X_{up} emission is located at 2.857 (3L), 2.712 (4L), 2.642 (5L), and 2.608 eV (6L), and the HX is located at 2.76 (3L) and 2.67 eV (4L) and 2.621 (5L). However, neither X_{up} nor HX emission is detected in 2L WSe₂. For clarity, we summarise the energies of X_{up} , X_D and $\Gamma\Gamma$ excitons (extracted from absorbance spectra) as a function of the number of layers in Fig. 2c. The X_{up} energies (filled blue circles) closely match the red dashed curve, which depicts twice the energy of X_D (labelled as $2 \times E_{XD}$), reinforcing that X_{up} is strongly correlated with X_D . Furthermore, the X_{up} energy moves toward $\Gamma\Gamma$ excitons (filled green triangles) with the increasing number of layers and overlaps $\Gamma\Gamma$ excitons beyond 5L WSe₂, resulting in a strongly enhanced light upconversion intensity evident in Figure 2b and quantified by the open blue triangles in Figure 2c. We found that upconversion efficiency Q_{up} (defined in Methods), is greater than unity in 5L WSe₂ and above, which is at least ten times higher than 3L WSe₂. The $Q_{up} > 1$ means that UPL emission is larger than X_D emission, quantitatively suggesting an efficient light upconversion occurred at the resonance between X_{up} and $\Gamma\Gamma$ excitons.

We believe that the efficient light conversion is a consequence of the resonant EEA process, as illustrated in Figure 3a. Upon optical excitation, photoexcited bright excitons thermally relax to X_D via multiple phonon scattering. X_D is the momentum-forbidden dark exciton with a finite centre of mass (CoM) momentum, leading to prolonged population lifetime up to tens of nanoseconds.^{38,39} The fact that X_D has orders of magnitude longer lifetime than bright excitons favours pronounced many-body interactions.^{40,41} In our case, the X_D is upconverted to a higher energy state X_{up} through EEA, followed by radiative recombination at an energy above the initial excitation. Notably, the UPL emission of X_{up}

suggests that the radiative recombination is favoured over phonon scattering as the relaxation pathway, which typically occurs on much shorter timescales of 10–100 fs.^{42–44} This indicates that the spontaneous emission holds a competitive edge in the dynamics of upconverted excitons in few-layer WSe₂.

We propose a model wherein a resonant EEA facilitates the light upconversion in few-layer WSe₂ (see more detail in **Supplementary note 2**). The resonant EEA process involves the initial state (dark excitons) upconverting to the final state (bright excitons) under a fundamental restriction—both states must follow the conservation of energy and momentum. Figure 3b illustrates a viable pathway for Q Γ dark excitons undergoing the resonant EEA upon the momentum-conserving principle. In the right panel, the final state entails that both electron and hole are at the Γ valley, where bright excitons exhibit zero CoM momentum. For this to occur, two X_D in the initial state (left panel) could be momentum-indirect with opposite momenta, a hole at Γ valley and an electron at Q/Q' valley. The EEA of such dark exciton pairs describes that one dark exciton recombines non-radiatively and transfers its energy and momentum to the other dark exciton, and that the electron of the other dark exciton originally occupying the lowest available conduction band (Q/Q' valley) is scattered to a high-lying conduction band, forming a bright exciton at Γ valley. We note that the EEA process is also possible by scattering the hole originally occupying the highest available valence band to a lower valence band, forming high-lying bright excitons at Q valley (see Supplementary Fig. 2b). Last, for the resonance to be achieved, the energy of the final state must be approximately twice of that of the initial state. Therefore, the energy conservation allows us to identify possible final states in subsequent calculations.

Figure 3c–e show the calculated exciton energies of dark X_D and bright excitons (Γ_{ex}) with different CoM momentum for 1L, 2L, and 4L WSe₂, respectively (see **Supplementary note 2** for detail). We consider bright exciton states observed in Figure 1 (KK_A, KK_B, QQ, and $\Gamma\Gamma$) and dark exciton states (K'K, QK, Q Γ , K Γ) that potentially fulfil the valley and band selection rules for the resonant EEA process. In order to identify available final states for involving in the resonant EEA, we depict the energy and the doubled energy of the lowest-lying dark excitons as the grey and light green bars in the figures respectively. For 1L WSe₂, the lowest energy QK excitons could upconvert to high-lying KK or QQ excitons, but only the high-lying KK excitons fulfil the resonance criterion. Our calculation also supports the recent experimental observation of UPL involving the high-lying KK excitons with negative effective mass and KK_A excitons.⁴⁵ For 2L WSe₂, the lowest energy QK excitons upconverting to $\Gamma\Gamma$ excitons does not obey the selection rule (The non-resonant process is denoted with a grey arrow with red X in Fig. 3d; see item 3 of Supplementary Table 1.), which explains the absence of light upconversion in our experiments (See black curve in Figure 2b). As the thickness increases, QK and Q Γ excitons become the lowest energy and are likely degenerate in 4L WSe₂, and a cluster of $\Gamma\Gamma$ excitons (green solid lines in Figure 3e) lies in the vicinity of twice the energy of Q Γ /QK excitons,

enabling efficient channels for the resonant EEA (denoted with red arrow in Fig. 3e). In the process of resonant EEA, a $Q\Gamma$ exciton is upconverted into $\Gamma\Gamma$ excitons by absorbing the energy and momentum of either a QK or a $Q'\Gamma$ exciton, which possesses an opposite momentum of the $Q\Gamma$ exciton (see items 4 and 6 of Supplementary Table 1). We note that only a fraction of $\Gamma\Gamma$ excitons within the double energy of dark excitons can contribute to the UPL.

Our power-dependent measurement further supports the mechanism of EEA-assisted light upconversion in few-layer WSe_2 . UPL spectra in 5L WSe_2 show that the overall intensity increases nonlinearly obtained with power density from 0.03 to 1.02 $mW/\mu m^2$ (see Extended Data Fig. 3a). We integrate the intensity of UPL (including X_{up} and HX) and plot it as a function of excitation power density in Figure 3f. Notably, the 5L WSe_2 sample exhibits a superlinear dependence with exponent $\alpha = 2$ below $P = 0.1 mW/\mu m^2$, suggesting an EEA behaviour. In contrast, bulk WSe_2 exhibits the power law exponent of $\alpha = 3$, suggesting the conventional Auger recombination (see the corresponding UPL spectra in Extended Data Fig. 3b). This fundamental difference demonstrates that the light upconversion via resonant EEA is inherently a low-dimensional phenomenon—the dominance of tightly bound excitons in few-layer WSe_2 due to the quantum confinement and the reduced dielectric screening, resulting in much higher exciton binding energies compared to the bulk counterpart. We note that the superlinear dependence of EEA can also be observed in other few-layer WSe_2 (see Extended Data Figs. 3c–h). Regardless of the layer thickness, we observed a saturation of UPL intensity approaching linear dependence at $P > 0.1 mW/\mu m^2$. The saturation may imply other higher-order nonlinear processes at elevating exciton density, which become significant at the specific power threshold. This highlights rich and intricate many-body dynamics under intense optical excitation. More dynamical studies are required to elucidate the interactions and relaxation of X_{up} , which may be critical for nonlinear optical and optoelectronic applications.

The resonant EEA is fundamentally different from other common upconversion mechanisms observed in other 2D materials, such as SHG and phonon-assisted upconversion. Figure 4a shows the evolution of UPL spectra in a 5L WSe_2 with various excitation energies (E_{in}). 5L WSe_2 has no inversion symmetry, allowing us to compare the EEA and SHG. We utilised a tuneable pulsed laser to selectively excite near resonantly with X_D at E_{in} from 1.24 to 1.33 eV. Emission energies in the spectra are fitted with two Gaussians (see Methods), as displayed in Figure 4b. In Figure 4a, across all the excitation energies, we observed an emission peak (yellow) strongly correlating with the E_{in} . The extracted peak energies show a good agreement with doubled excitation energy, $2 \times E_{in}$ (depicted as the grey solid line in Figure 4b), indicating a SHG characteristic. Remarkably, when the excitation energy was tuned closely to the energy of X_D peak (1.301–1.326 eV), an additional emission peak (blue) appears at 2.575 eV, which we identified as UPL, is nearly independent of E_{in} (denoted as X_{up} in Figure 4b). This

independence is distinct from the SHG peaks because the UPL is only present at E_{in} near the dark exciton energy, whereas SHG signal is observed throughout the excitation energies. We further depict normalised UPL intensity as a function of the excitation energy in Figure 4c. The intensity is significant at 1.28 eV but negligible at both 1.24 and 1.33 eV, indicating the correlation between the UPL intensity and the population of dark excitons. Second, Figure 4d shows the UPL peaks in both HH (co-polarisation) and HV (cross-polarisation) configurations⁴⁶ (see Methods for more detail). The UPL intensity is identical in different polarisation configurations, in contrast to the SHG in which the inherently polarisation-dependent process is described by the tensor of second-order nonlinear optical susceptibility.⁴⁷ Third, SHG often necessitates a femtosecond pulsed laser to achieve high photon density. Our experiments, however, have demonstrated the pronounced UPL signal simply using a CW laser, suggesting a low threshold of photon density in the upconversion process. Fourth, in contrast to SHG which only present in odd-layer samples due to the broken inversion symmetry, UPL is persistently present for WSe₂ thickness beyond 3 layers without any evident odd/even layer dependence, as we already demonstrated in Figure 2. All the above observations point to the importance of the dark exciton in UPL and ruling out SHG as the primary mechanism for light upconversion.

The phonon-assisted upconversion is a mechanism through which extra energy is provided to excitons through exciton-phonon interactions, resulting in a transition to higher excitonic states.^{28,48} As a result, the increasing temperature tends to increase the phonon population and thus enhance upconversion process. Figure 4e shows UPL intensity of 5L WSe₂ sample as a function of temperature. The UPL remains detectable up to room temperature while the intensity exponentially decreases as the temperature increases, which cannot be explained by the phonon-assisted process. Moreover, the energy difference between UPL emission and excitation energy is significantly higher than the energy of optical phonons in 5L WSe₂, which is about 50 meV (see Extended Data Fig. 4). These observations support the unlikelihood of phonon-assisted upconversion playing a role in our observations.

The light upconversion is not exclusive to few-layer WSe₂, but seen in few-layer WS₂, MoS₂, and MoSe₂. Figure 5a shows that the UPL emission (2.875 eV for 5L WS₂, 2.77 eV for 3L MoS₂, and 2.49 eV for 3L MoSe₂) closely matches the double energy of the dark exciton emissions (1.43 eV for 5L WS₂, 1.4 eV for 3L MoS₂, and 1.28 eV for 3L MoSe₂), signifying the important role of dark excitons in the light upconversion. Figure 5b shows that UPL intensity is strongly enhanced as the layer thickness increases, suggesting a shared characteristic of the resonant EEA process within the few-layer (Mo, W)(S, Se)₂. Moreover, we highlight that the UPL emission is tuneable, offering a significant advantage for applications requiring specific wavelengths. Figure 5c summarises the peak energy of UPL in few-layer WSe₂, WS₂, MoS₂, and MoSe₂. The UPL emission energies span a broad spectrum, ranging from green light (2.34 eV) to ultraviolet light (3.1 eV). Such tunability illustrates the potential of these

materials in enhancing optoelectronic and photocatalytic applications through engineered light-matter interactions.

In summary, our research has showcased efficient light upconversion in atomically thin TMDs. The UPL is driven by the resonant EEA of momentum-indirect dark excitons. The demonstrated many-body interaction provides a universal route for harnessing the energy of the lowest-lying momentum-indirect excitons to generate green to ultraviolet light, featuring a broad scope of tunability. The process of exciton-mediated light conversion underlines the intricate many-body excitonic physics within TMDs and opens a door to promising advancements in the fields of optoelectronics and photocatalysis, where control over such fundamental interactions is essential.

REFERENCES (UP TO 50)

- (1) DaCosta, M. V.; Doughan, S.; Han, Y.; Krull, U. J. Lanthanide Upconversion Nanoparticles and Applications in Bioassays and Bioimaging: A Review. *Anal. Chim. Acta* **2014**, *832*, 1–33. <https://doi.org/10.1016/j.aca.2014.04.030>.
- (2) Wang, M.; Abbineni, G.; Clevenger, A.; Mao, C.; Xu, S. Upconversion Nanoparticles: Synthesis, Surface Modification and Biological Applications. *Nanomedicine Nanotechnol. Biol. Med.* **2011**, *7* (6), 710–729. <https://doi.org/10.1016/j.nano.2011.02.013>.
- (3) Borse, S.; Rafique, R.; P. Murthy, Z. V.; Jung Park, T.; Kumar Kailasa, S. Applications of Upconversion Nanoparticles in Analytical and Biomedical Sciences: A Review. *Analyst* **2022**, *147* (14), 3155–3179. <https://doi.org/10.1039/D1AN02170B>.
- (4) Chen, G.; Qiu, H.; Prasad, P. N.; Chen, X. Upconversion Nanoparticles: Design, Nanochemistry, and Applications in Theranostics. *Chem. Rev.* **2014**, *114* (10), 5161–5214. <https://doi.org/10.1021/cr400425h>.
- (5) Wang, F.; Banerjee, D.; Liu, Y.; Chen, X.; Liu, X. Upconversion Nanoparticles in Biological Labeling, Imaging, and Therapy. *Analyst* **2010**, *135* (8), 1839–1854. <https://doi.org/10.1039/C0AN00144A>.
- (6) Richards, B. S.; Hudry, D.; Busko, D.; Turshatov, A.; Howard, I. A. Photon Upconversion for Photovoltaics and Photocatalysis: A Critical Review. *Chem. Rev.* **2021**, *121* (15), 9165–9195. <https://doi.org/10.1021/acs.chemrev.1c00034>.
- (7) F. Schulze, T.; W. Schmidt, T. Photochemical Upconversion: Present Status and Prospects for Its Application to Solar Energy Conversion. *Energy Environ. Sci.* **2015**, *8* (1), 103–125. <https://doi.org/10.1039/C4EE02481H>.
- (8) Syroeshkin, M. A.; Kuriakose, F.; Saverina, E. A.; Timofeeva, V. A.; Egorov, M. P.; Alabugin, I. V. Upconversion of Reductants. *Angew. Chem. Int. Ed.* **2019**, *58* (17), 5532–5550. <https://doi.org/10.1002/anie.201807247>.
- (9) Zhou, B.; Shi, B.; Jin, D.; Liu, X. Controlling Upconversion Nanocrystals for Emerging Applications. *Nat. Nanotechnol.* **2015**, *10* (11), 924–936. <https://doi.org/10.1038/nnano.2015.251>.
- (10) Wang, Q.; Wee, A. T. S. Photoluminescence Upconversion of 2D Materials and Applications. *J. Phys. Condens. Matter* **2021**, *33* (22), 223001. <https://doi.org/10.1088/1361-648X/abf37f>.
- (11) Tian, Q.; Yao, W.; Wu, W.; Jiang, C. NIR Light-Activated Upconversion Semiconductor Photocatalysts. *Nanoscale Horiz.* **2019**, *4* (1), 10–25. <https://doi.org/10.1039/C8NH00154E>.
- (12) Yin, H.-J.; Xiao, Z.-G.; Feng, Y.; Yao, C.-J. Recent Progress in Photonic Upconversion Materials for Organic Lanthanide Complexes. *Materials* **2023**, *16* (16), 5642. <https://doi.org/10.3390/ma16165642>.
- (13) Singh-Rachford, T. N.; Castellano, F. N. Photon Upconversion Based on Sensitized Triplet–Triplet Annihilation. *Coord. Chem. Rev.* **2010**, *254* (21), 2560–2573. <https://doi.org/10.1016/j.ccr.2010.01.003>.

- (14) Ansari, A. A.; Nazeeruddin, M. K.; Tavakoli, M. M. Organic-Inorganic Upconversion Nanoparticles Hybrid in Dye-Sensitized Solar Cells. *Coord. Chem. Rev.* **2021**, *436*, 213805. <https://doi.org/10.1016/j.ccr.2021.213805>.
- (15) Brett, M. W.; Gordon, C. K.; Hardy, J.; Davis, N. J. L. K. The Rise and Future of Discrete Organic–Inorganic Hybrid Nanomaterials. *ACS Phys. Chem. Au* **2022**, *2* (5), 364–387. <https://doi.org/10.1021/acspyschemau.2c00018>.
- (16) Seo, S. E.; Choe, H.-S.; Cho, H.; Kim, H.; Kim, J.-H.; Kwon, O. S. Recent Advances in Materials for and Applications of Triplet–Triplet Annihilation-Based Upconversion. *J. Mater. Chem. C* **2022**, *10* (12), 4483–4496. <https://doi.org/10.1039/D1TC03551G>.
- (17) C. Simon, Y.; Weder, C. Low-Power Photon Upconversion through Triplet–Triplet Annihilation in Polymers. *J. Mater. Chem.* **2012**, *22* (39), 20817–20830. <https://doi.org/10.1039/C2JM33654E>.
- (18) Korkusinski, M.; Voznyy, O.; Hawrylak, P. Theory of Highly Excited Semiconductor Nanostructures Including Auger Coupling: Exciton-Biexciton Mixing in CdSe Nanocrystals. *Phys. Rev. B* **2011**, *84* (15), 155327. <https://doi.org/10.1103/PhysRevB.84.155327>.
- (19) Ma, Y.-Z.; Valkunas, L.; Dexheimer, S. L.; Bachilo, S. M.; Fleming, G. R. Femtosecond Spectroscopy of Optical Excitations in Single-Walled Carbon Nanotubes: Evidence for Exciton-Exciton Annihilation. *Phys. Rev. Lett.* **2005**, *94* (15), 157402. <https://doi.org/10.1103/PhysRevLett.94.157402>.
- (20) Abakumov, V. N.; Perel, V. I.; Yassievich, I. N. *Nonradiative Recombination in Semiconductors*; Elsevier, 1991.
- (21) Mak, K. F.; Shan, J. Photonics and Optoelectronics of 2D Semiconductor Transition Metal Dichalcogenides. *Nat. Photonics* **2016**, *10* (4), 216–226. <https://doi.org/10.1038/nphoton.2015.282>.
- (22) Ma, X.; Roslyak, O.; Duque, J. G.; Pang, X.; Doorn, S. K.; Piryatinski, A.; Dunlap, D. H.; Htoon, H. Influences of Exciton Diffusion and Exciton-Exciton Annihilation on Photon Emission Statistics of Carbon Nanotubes. *Phys. Rev. Lett.* **2015**, *115* (1), 017401. <https://doi.org/10.1103/PhysRevLett.115.017401>.
- (23) Soavi, G.; Dal Conte, S.; Manzoni, C.; Viola, D.; Narita, A.; Hu, Y.; Feng, X.; Hohenester, U.; Molinari, E.; Prezzi, D.; Müllen, K.; Cerullo, G. Exciton–Exciton Annihilation and Biexciton Stimulated Emission in Graphene Nanoribbons. *Nat. Commun.* **2016**, *7* (1), 11010. <https://doi.org/10.1038/ncomms11010>.
- (24) Akselrod, G. M.; Tischler, Y. R.; Young, E. R.; Nocera, D. G.; Bulovic, V. Exciton-Exciton Annihilation in Organic Polariton Microcavities. *Phys. Rev. B* **2010**, *82* (11), 113106. <https://doi.org/10.1103/PhysRevB.82.113106>.
- (25) Xu, Z.; Huang, Z.; Jin, T.; Lian, T.; Tang, M. L. Mechanistic Understanding and Rational Design of Quantum Dot/Mediator Interfaces for Efficient Photon Upconversion. *Acc. Chem. Res.* **2021**, *54* (1), 70–80. <https://doi.org/10.1021/acs.accounts.0c00526>.
- (26) Lee, K. J.; Xin, W.; Guo, C. Annihilation Mechanism of Excitons in a MoS₂ Monolayer through Direct Förster-Type Energy Transfer and Multistep Diffusion. *Phys. Rev. B* **2020**, *101* (19), 195407. <https://doi.org/10.1103/PhysRevB.101.195407>.

- (27) Mouri, S.; Miyauchi, Y.; Toh, M.; Zhao, W.; Eda, G.; Matsuda, K. Nonlinear Photoluminescence in Atomically Thin Layered WSe₂ Arising from Diffusion-Assisted Exciton-Exciton Annihilation. *Phys. Rev. B* **2014**, *90* (15), 155449. <https://doi.org/10.1103/PhysRevB.90.155449>.
- (28) Jadcak, J.; Bryja, L.; Kutrowska-Girzycka, J.; Kapuściński, P.; Bieniek, M.; Huang, Y.-S.; Hawrylak, P. Room Temperature Multi-Phonon Upconversion Photoluminescence in Monolayer Semiconductor WS₂. *Nat. Commun.* **2019**, *10* (1), 107. <https://doi.org/10.1038/s41467-018-07994-1>.
- (29) Niu, Y.; Gonzalez-Abad, S.; Frisenda, R.; Marauhn, P.; Drüppel, M.; Gant, P.; Schmidt, R.; Taghavi, N. S.; Barcons, D.; Molina-Mendoza, A. J.; De Vasconcellos, S. M.; Bratschitsch, R.; Perez De Lara, D.; Rohlfing, M.; Castellanos-Gomez, A. Thickness-Dependent Differential Reflectance Spectra of Monolayer and Few-Layer MoS₂, MoSe₂, WS₂ and WSe₂. *Nanomaterials* **2018**, *8* (9), 725. <https://doi.org/10.3390/nano8090725>.
- (30) Kozawa, D.; Kumar, R.; Carvalho, A.; Kumar Amara, K.; Zhao, W.; Wang, S.; Toh, M.; Ribeiro, R. M.; Castro Neto, A. H.; Matsuda, K.; Eda, G. Photocarrier Relaxation Pathway in Two-Dimensional Semiconducting Transition Metal Dichalcogenides. *Nat. Commun.* **2014**, *5* (1), 4543. <https://doi.org/10.1038/ncomms5543>.
- (31) Wang, L.; Wang, Z.; Wang, H.-Y.; Grinblat, G.; Huang, Y.-L.; Wang, D.; Ye, X.-H.; Li, X.-B.; Bao, Q.; Wee, A.-S.; Maier, S. A.; Chen, Q.-D.; Zhong, M.-L.; Qiu, C.-W.; Sun, H.-B. Slow Cooling and Efficient Extraction of C-Exciton Hot Carriers in MoS₂ Monolayer. *Nat. Commun.* **2017**, *8* (1), 13906. <https://doi.org/10.1038/ncomms13906>.
- (32) Bieniek, M.; Korkusiński, M.; Szulakowska, L.; Potasz, P.; Ozfidan, I.; Hawrylak, P. Band Nesting, Massive Dirac Fermions, and Valley Landé and Zeeman Effects in Transition Metal Dichalcogenides: A Tight-Binding Model. *Phys. Rev. B* **2018**, *97* (8), 085153. <https://doi.org/10.1103/PhysRevB.97.085153>.
- (33) Lindlau, J.; Selig, M.; Neumann, A.; Colombier, L.; Förste, J.; Funk, V.; Förg, M.; Kim, J.; Berghäuser, G.; Taniguchi, T.; Watanabe, K.; Wang, F.; Malic, E.; Högele, A. The Role of Momentum-Dark Excitons in the Elementary Optical Response of Bilayer WSe₂. *Nat. Commun.* **2018**, *9* (1), 2586. <https://doi.org/10.1038/s41467-018-04877-3>.
- (34) Kim, H.; Choi, H. J. Thickness Dependence of Work Function, Ionization Energy, and Electron Affinity of Mo and W Dichalcogenides from DFT and GW Calculations. *Phys. Rev. B* **2021**, *103* (8), 085404. <https://doi.org/10.1103/PhysRevB.103.085404>.
- (35) Radiative Transitions between Discrete States in Atomic Systems. In *Radiative Processes in Atomic Physics*; John Wiley & Sons, Ltd, 1997; pp 61–118. <https://doi.org/10.1002/3527605606.ch2>.
- (36) Hong, J.; Senga, R.; Pichler, T.; Suenaga, K. Probing Exciton Dispersions of Freestanding Monolayer WSe₂ by Momentum-Resolved Electron Energy-Loss Spectroscopy. *Phys. Rev. Lett.* **2020**, *124* (8), 087401. <https://doi.org/10.1103/PhysRevLett.124.087401>.
- (37) Zhao, W.; Ribeiro, R. M.; Toh, M.; Carvalho, A.; Kloc, C.; Neto, A. H. C.; Eda, G. *Origin of Indirect Optical Transitions in Few-Layer MoS₂, WS₂, and WSe₂*. ACS Publications. <https://doi.org/10.1021/nl403270k>.

- (38) Mondal, N.; Azam, N.; Gartstein, Y. N.; Mahjouri-Samani, M.; Malko, A. V. Photoexcitation Dynamics and Long-Lived Excitons in Strain-Engineered Transition Metal Dichalcogenides. *Adv. Mater.* **2022**, *34* (23), 2110568. <https://doi.org/10.1002/adma.202110568>.
- (39) Liu, H.; Pau, A.; Efimkin, D. K. Hybrid Dark Excitons in Monolayer MoS₂. *Phys. Rev. B* **2021**, *104* (16), 165411. <https://doi.org/10.1103/PhysRevB.104.165411>.
- (40) Wierzbowski, J.; Klein, J.; Sigger, F.; Straubinger, C.; Kremser, M.; Taniguchi, T.; Watanabe, K.; Wurstbauer, U.; Holleitner, A. W.; Kaniber, M.; Müller, K.; Finley, J. J. Direct Exciton Emission from Atomically Thin Transition Metal Dichalcogenide Heterostructures near the Lifetime Limit. *Sci. Rep.* **2017**, *7* (1), 12383. <https://doi.org/10.1038/s41598-017-09739-4>.
- (41) Ajayi, O. A.; Ardelean, J. V.; Shepard, G. D.; Wang, J.; Antony, A.; Taniguchi, T.; Watanabe, K.; Heinz, T. F.; Strauf, S.; Zhu, X.-Y.; Hone, J. C. Approaching the Intrinsic Photoluminescence Linewidth in Transition Metal Dichalcogenide Monolayers. *2D Mater.* **2017**, *4* (3), 031011. <https://doi.org/10.1088/2053-1583/aa6aa1>.
- (42) Selig, M.; Berghäuser, G.; Richter, M.; Bratschitsch, R.; Knorr, A.; Malic, E. Dark and Bright Exciton Formation, Thermalization, and Photoluminescence in Monolayer Transition Metal Dichalcogenides. *2D Mater.* **2018**, *5* (3), 035017. <https://doi.org/10.1088/2053-1583/aabea3>.
- (43) Kaasbjerg, K.; Thygesen, K. S.; Jacobsen, K. W. Phonon-Limited Mobility in n-Type Single-Layer MoS₂ from First Principles. *Phys. Rev. B* **2012**, *85* (11), 115317. <https://doi.org/10.1103/PhysRevB.85.115317>.
- (44) Wallauer, R.; Reimann, J.; Armbrust, N.; Gütde, J.; Höfer, U. Intervalley Scattering in MoS₂ Imaged by Two-Photon Photoemission with a High-Harmonic Probe. *Appl. Phys. Lett.* **2016**, *109* (16), 162102. <https://doi.org/10.1063/1.4965839>.
- (45) Lin, K.-Q.; Ong, C. S.; Bange, S.; Faria Junior, P. E.; Peng, B.; Ziegler, J. D.; Zipfel, J.; Bäuml, C.; Paradiso, N.; Watanabe, K.; Taniguchi, T.; Strunk, C.; Monserrat, B.; Fabian, J.; Chernikov, A.; Qiu, D. Y.; Louie, S. G.; Lupton, J. M. Narrow-Band High-Lying Excitons with Negative-Mass Electrons in Monolayer WSe₂. *Nat. Commun.* **2021**, *12* (1), 5500. <https://doi.org/10.1038/s41467-021-25499-2>.
- (46) Chen, S.-Y.; Goldstein, T.; Venkataraman, D.; Ramasubramaniam, A.; Yan, J. Activation of New Raman Modes by Inversion Symmetry Breaking in Type II Weyl Semimetal Candidate T'-MoTe₂. *Nano Lett.* **2016**, *16* (9), 5852–5860. <https://doi.org/10.1021/acs.nanolett.6b02666>.
- (47) Autere, A.; Jussila, H.; Dai, Y.; Wang, Y.; Lipsanen, H.; Sun, Z. Nonlinear Optics with 2D Layered Materials. *Adv. Mater.* **2018**, *30* (24), 1705963. <https://doi.org/10.1002/adma.201705963>.
- (48) Jones, A. M.; Yu, H.; Schaibley, J. R.; Yan, J.; Mandrus, D. G.; Taniguchi, T.; Watanabe, K.; Dery, H.; Yao, W.; Xu, X. Excitonic Luminescence Upconversion in a Two-Dimensional Semiconductor. *Nat. Phys.* **2016**, *12* (4), 323–327. <https://doi.org/10.1038/nphys3604>.
- (49) Liu, S.; Liu, Y.; Holtzman, L.; Li, B.; Holbrook, M.; Pack, J.; Taniguchi, T.; Watanabe, K.; Dean, C. R.; Pasupathy, A. N.; Barmak, K.; Rhodes, D. A.; Hone, J. Two-Step Flux Synthesis of Ultrapure Transition-Metal Dichalcogenides. *ACS Nano* **2023**, *17* (17), 16587–16596. <https://doi.org/10.1021/acsnano.3c02511>.

METHODS

Samples preparation

Bulk WSe₂ and MoSe₂ crystals with ultra-low defects were grown by a two-step self-flux method.⁴⁹ The bulk WS₂ and MoS₂ crystals were purchased from HQ Graphene and SPI supplies, respectively. Thin TMD flakes were mechanically exfoliated onto polydimethylsiloxane (PDMS) and subsequently dry-transferred onto Al₂O₃ or SiO₂/Si substrates. The layer thickness of the samples was determined by analysing optical contrast and ultra-low frequency Raman spectroscopy, as shown in **Extended Data Fig. 1**.

Upconversion Photoluminescence Spectroscopy

The fresh-made samples are transferred to a cryostat with optical access (Janis ST-500) under a high-vacuum environment (base pressure $< 5 \times 10^{-6}$ Torr) to ensure reliable results. The sample can be cooled down to 80 K by continuous flowing liquid nitrogen. A diode-pump solid-state continuous-wave laser at an excitation energy of 2.33 and 1.96 eV was employed for excitation. The spectroscopy was set up in a back-scattering configuration. A 40 \times objective lens (numerical aperture, 0.6) was applied to focus the laser to the diffraction limit. The PL signal was filtered by three cascaded Bragg notch filters (OptiGrate), dispersed by a grating-based monochromator (Horiba, iHR-550 with 150 gr/mm grating), and detected by a nitrogen-cooled charge-coupled device (Horiba, Symphony II). In addition, two linear polarisers are placed in incident and scattered light, which enable us to select polarisation of incident/scattered light and the relative polarisation between them. In Fig. 4d, the 0 $^\circ$ and 90 $^\circ$ of relative polarisation is defined as parallel (HH) and perpendicular (HV) mode, respectively. Note that all experimental figures are executed at a temperature of 80 K and incident power of 0.34 mW/ μm^2 unless stated.

Ultrafast Photoluminescence Spectroscopy

The ultrafast photoluminescence spectroscopy with tuneable fs pulses was executed with samples at $T = 9$ K in a closed-cycle cryostat (Montana Instruments, Cryostation). A 20 \times objective lens (numerical aperture, 0.38) was used both to focus the excitation laser and collect the PL emission. The tuneable excitation came from a non-collinear optical parametric amplifier (Light Conversion, Orpheus-N-3H) pumped by the third harmonic of a Nd:YAG amplified femtosecond laser system (Light Conversion, Pharos). The spectrum of each excitation pulse was measured before the sample by a Thorlabs CCS200 spectrometer. The PL emission was separated from the pump by a 600 nm short-pass dichroic beam splitter, and measured using an Andor Kymera 328i spectrometer with an Andor Zyla sCMOS camera.

The recorded spectra were processed using a custom written python script. Each peak was fit by two Gaussian functions: one for the PL emission component and the other for the SHG component. The fits were completed using the SciPy Curve Fit module. The peak energy and full-width at half-maximum (FWHM) of the SHG component were fixed, based on the parameters from a Gaussian fit of the excitation spectrum. Specifically, the peak energy was determined by doubling the energy and the FWHM was scaled by a factor of $\sqrt{2}$ from the values obtained for the excitation spectrum. The integrated peak amplitude of the PL emission was determined from the Gaussian fit parameters.

Normalisation of photoluminescence spectra and calculation of upconversion efficiency (Q_{up})

The PL spectra of 2–6L WSe₂ in Fig. 2a,b are normalised to 3L WSe₂ and the calculation of upconversion efficiency (Q_{up}) is based on the normalisation. Specifically, in Fig. 2a, we first calculated the integrated PL intensity of dark excitons for each layer thickness. The intensity ratio of each layer thickness to 3L WSe₂ can be calculated using $I_{\text{XD},n}/I_{\text{XD},3}$, where $I_{\text{XD},n}$ is the integrated PL intensity of dark excitons in n -layer WSe₂ ($n = 2-6$). The spectrum of 2–6L WSe₂ is then scaled according to the intensity ratio. In Fig. 2b, the same intensity ratio is applied to the UPL spectrum of 2–6L WSe₂. After the normalisation, we define the Q_{up} by counting the intensity ratio of UPL to the dark exciton PL, $(I_{\text{Xup}}+I_{\text{HX}})/I_{\text{XD}}$, where I_{Xup} , I_{HX} , and I_{XD} are integrated PL intensities of upconverted, high-lying, and dark excitons, respectively.

Author Contributions

Y. H. C. and P. Y. L. contribute equally to this work. Y. H. C. and S. Y. C. conceived and designed this project. Y. H. C. and S. Y. C. conducted device fabrication, optical measurement, and data analysis. J. H., L. N. H., and K. B. from Columbia University provided bulk WSe₂ and MoSe₂ crystals. M. H. contributed towards confirming the quality of TMD crystals. K. B. from Swinburne University of Technology conducted ultrafast optical measurement. P. Y. L., G. H. P., C. J. H., C. E. H., Y. N. H., P. H., H. C. H., and S. J. C. contributed theoretical calculations. W. H. W. provided resources for conducting optical measurements. The manuscript was written through contributions of all authors. All authors have given approval to the final version of the manuscript.

Notes

The authors declare no competing interest.

ACKNOWLEDGMENT

Tungsten diselenide and molybdenum diselenide crystal growth was supported under the United States National Science Foundation Materials Research Science and Engineering Center through grants DMR-1420634 and DMR-2011738. Y. H. Chen, K.W. Boschen, J. A. Davis, M. S. Fuhrer, and S.-Y. Chen acknowledge support from the ARC Centre of Excellence in Future Low-Energy Electronics Technologies (FLEET; CE170100039). S.-Y. Chen acknowledges support from the National Science and Technology Council of Taiwan through Grant 111-2112-M-002-047 and 112-2628-M-002-008-, and the Center of Atomic Initiative for New Materials, National Taiwan University (grant nos. 112 L9008 and 113 L9008), from the Featured Areas Research Center Program within the framework of the Higher Education Sprout Project by the Ministry of Education of Taiwan. S.-Y. Chen thanks the experimental support from Dr. Wei-Hua Wang in the Institute of Atomic and Molecular Sciences, Academia Sinica. S. J. Cheng acknowledges that this study is supported by the National Science and Technology Council of Taiwan under the contract, 112-2112-M-A49-028-, and by National Center for

High-Performance Computing of Taiwan. P. Y. Lo acknowledges support from the National Science and Technology Council of Taiwan, under the contract NSTC 112-2112-M-A49-019-MY3. H. C. Hsueh, C. E. Hsu, and Y. N. Hsu acknowledge the support from National Science and Technology Council, Taiwan, under Grant: 110-2112-M-032-014-MY3, and thank the National Center for High-Performance Computing in Taiwan for providing computational resources. P. H. work was supported by the Quantum Sensors QSP078 and On-Chip Integrated Photonic Circuits Based on 2D Materials HTSN341 Challenge Programs at the National Research Council of Canada, NSERC Discovery Grant No. RGPIN-2019-05714, and University of Ottawa Research Chair in Quantum Theory of Materials, Nanostructures, and Devices.

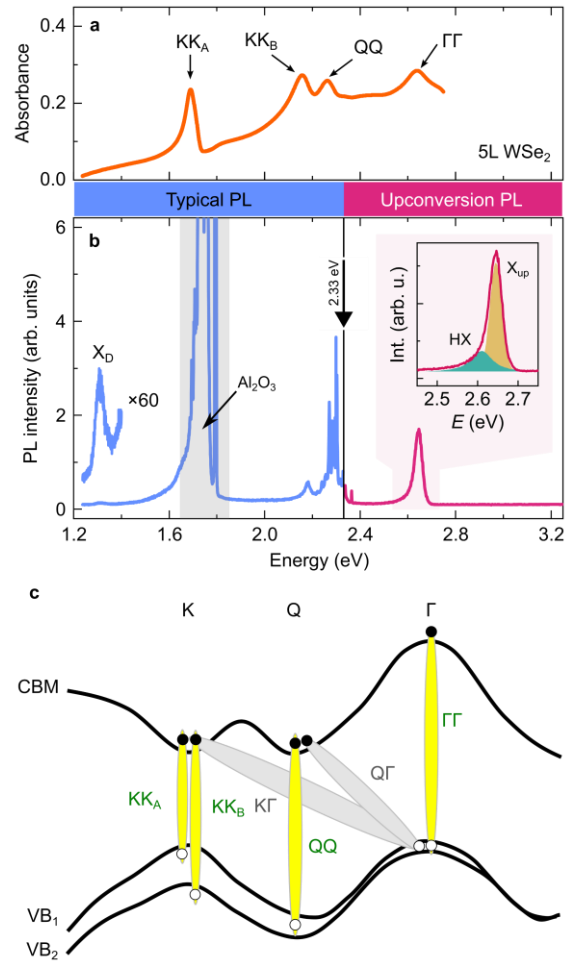


Figure 1. Bright, dark and upconverted excitons in 5L WSe₂. **(a)** Absorbance spectrum at $T = 80$ K with bright excitons indicated by arrows; labels discussed in text. **(b)** PL spectrum at $T = 80$ K excited with excitation energy 2.33 eV (wavelength 532 nm). The spectrum is divided into typical (blue) and upconversion PL (ruby) regimes. The inset in upconversion PL regime: The peak fittings of UPL from upconverted excitons X_{up} and high-lying excitons (HX). The low-energy PL is also shown magnified 60× to better show the dark exciton X_D emission at 1.31 eV. The grey shadow area indicates photoluminescence from the Al₂O₃ substrate. **(c)** The schematic of electronic band structure and corresponding bright/dark excitons observed in **(a,b)**.

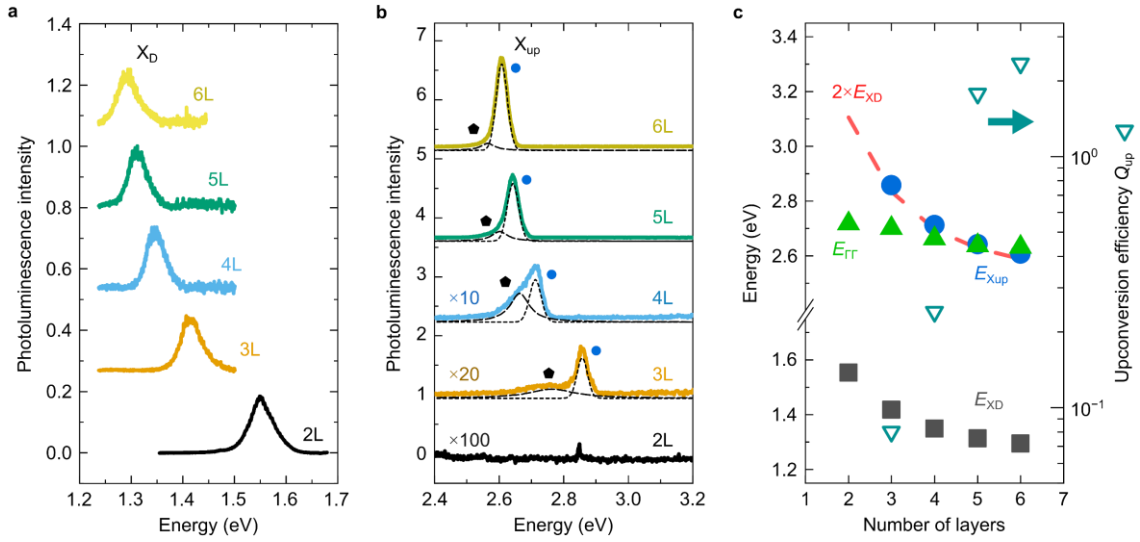


Figure 2. Layer-dependent characteristics of UPL in few-layer WSe₂ at $T = 80$ K. Evolution of **(a)** dark excitons X_D and **(b)** UPL spectra with the number of layers from 2L to 6L. The UPL emission of 3–6L WSe₂ can be deconvoluted into upconverted X_{up} (short dash line; peak denoted by circles) and high-lying excitons HX (long dash line; peak denoted by pentagons). The spectrum of each thickness is vertically shifted for clarity. **(c)** Emission energy of X_D and X_{up}, and absorption energy of $\Gamma\Gamma$ excitons $E_{\Gamma\Gamma}$, and extracted upconversion efficiency Q_{up} as a function of layer thickness. In **(a–c)**, the photoluminescence intensity is normalised to X_D emission of 3L WSe₂ (see Method for further details).

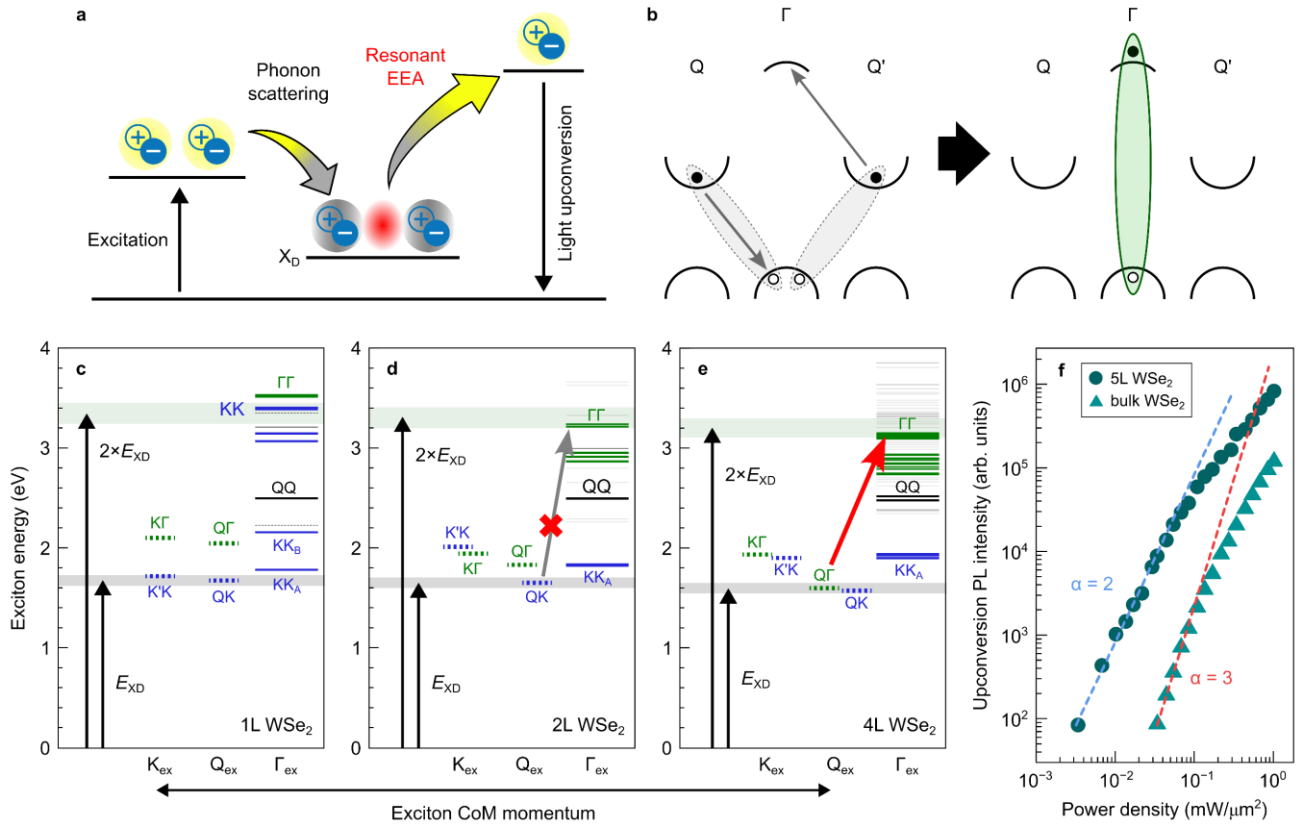


Figure 3. Resonant exciton-exciton annihilation of dark excitons in few-layer WSe₂. **(a)** The schematic of upconversion process in few-layer WSe₂. Light-excited bright excitons thermally relax to dark exciton states at the lowest energy X_D through multiple phonon scattering. The resonant EEA process upconverts two excitons X_D to a single high-energy exciton X_{up} , followed by a radiative combination, resulting in the light upconversion emission. **(b)** A schematic representation of excitonic upconversion before (left panel) and after the electron-scattering process (right panel). **(c–e)** Exciton energy as a function of exciton centre of mass (CoM) momentum in 1L **(c)**, 2L **(d)**, and 4L WSe₂ **(e)**. Black arrows denote the energy of the lowest energy dark exciton E_{XD} and the corresponding twice energy $2 \times E_{XD}$, respectively. **(f)** UPL intensity as a function of power density for 5L and bulk WSe₂ obtained at $T = 80$ K. The blue and red dash lines represent a power-law exponent $\alpha = 2$ and $\alpha = 3$, respectively.

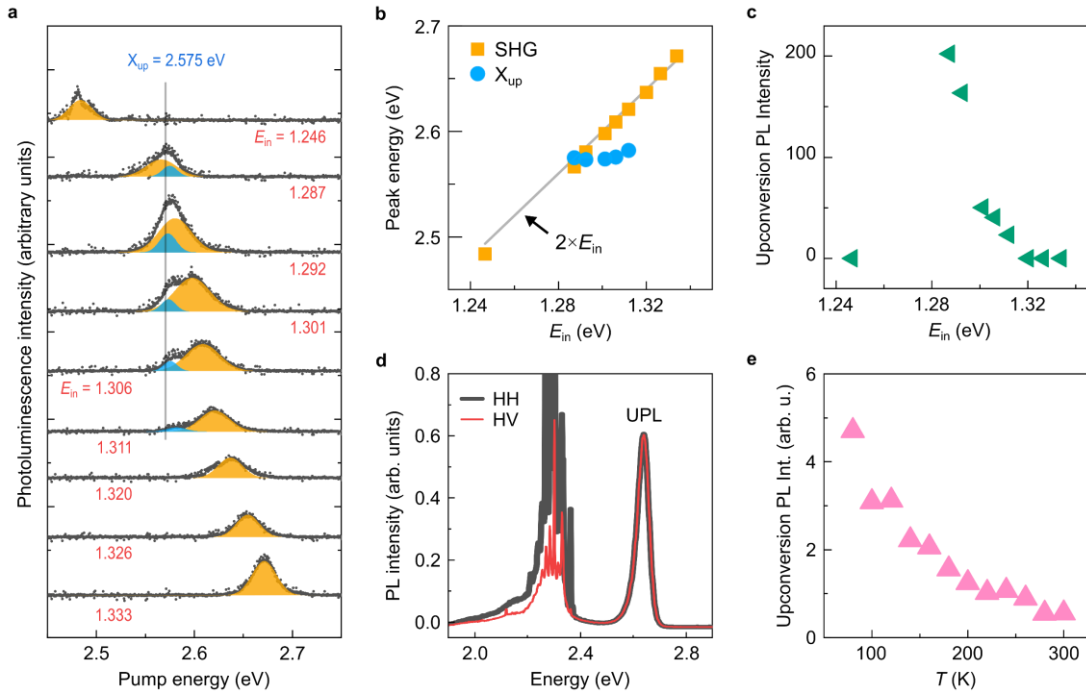


Figure 4. Excitation energy, polarisation, and temperature dependence of light upconversion in 5L WSe₂. **(a)** Evolution of UPL spectrum at $T = 9$ K with excitation energy from 1.246 to 1.333 eV. The excitation energy for each spectrum is labelled accordingly. Blue and orange peaks represent UPL emission from upconverted excitons X_{up} at 2.575 eV and SHG, respectively. **(b)** Extracted energy of X_{up} and SHG as a function of excitation energy. The grey solid line indicates the double of the excitation energy. **(c)** Normalised UPL intensity as a function of excitation energy obtained. The intensity is normalised by the square of incident power. **(d)** UPL spectra at $T = 80$ K obtained in perpendicular (HV) and parallel (HH) scattering configuration. **(e)** UPL intensity as a function of temperature ranging from 80 to 300 K.

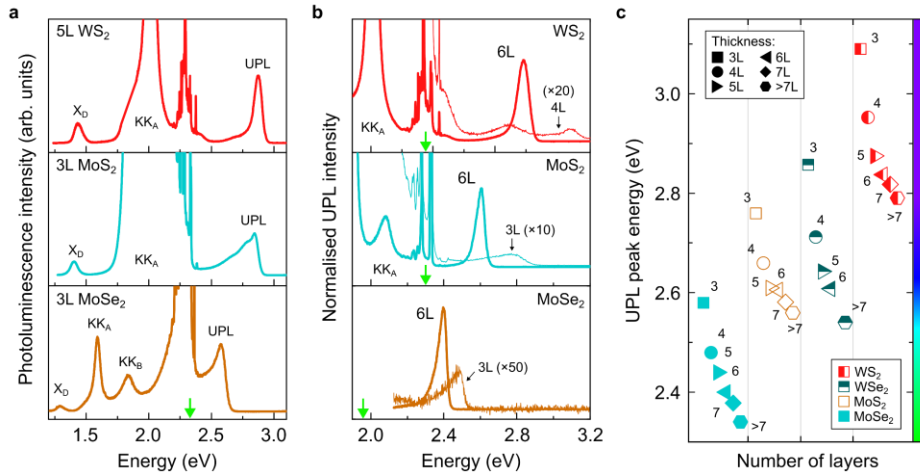
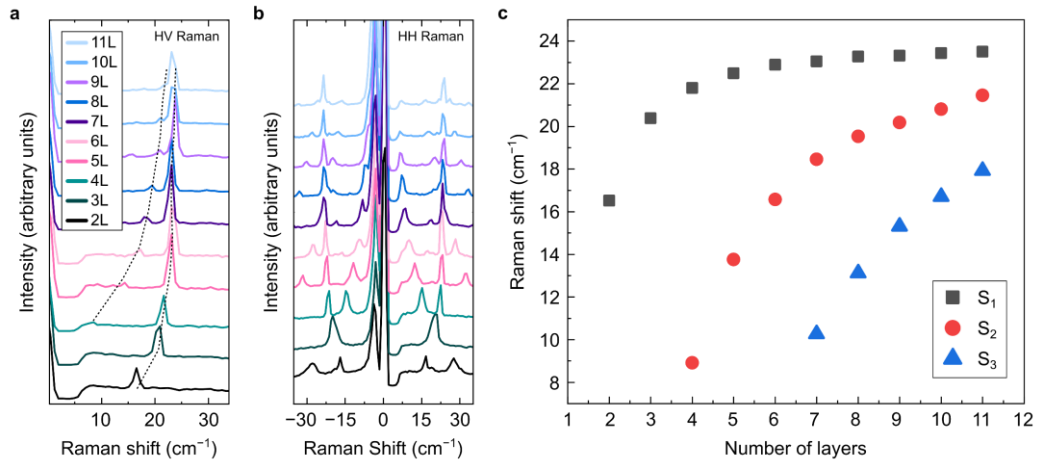
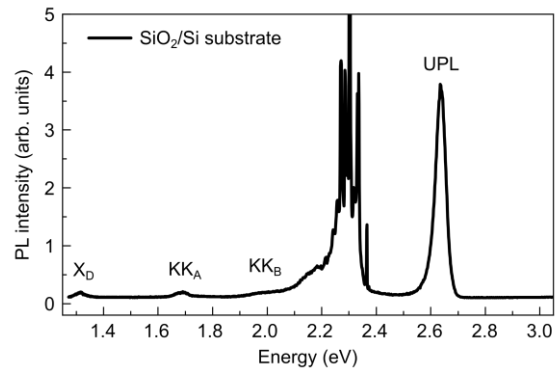


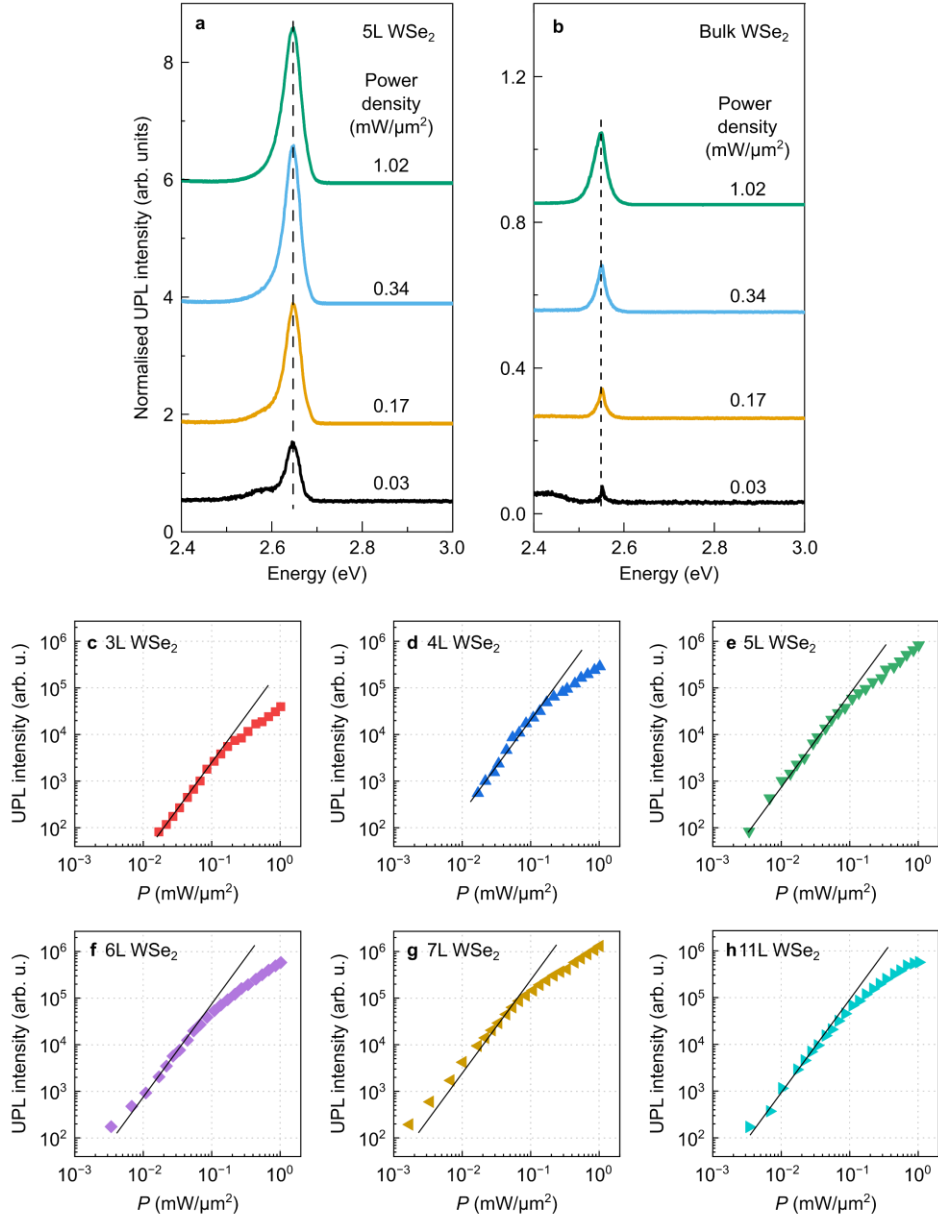
Figure 5. Light upconversion in few-layer MoS₂, MoSe₂, WS₂, and WSe₂ at $T = 80$ K. **(a)** Photoluminescence spectrum of 5L WS₂, 3L MoS₂, and 3L MoSe₂ at emission energy ranging from 1.2 to 3.1 eV. The excitation energy (2.33 eV) is denoted as the green arrow. **(b)** The UPL spectrum of 6L WS₂, MoS₂, and MoSe₂ in contrast to thinner counterparts (3L WS₂, 3L MoS₂, and 4L MoSe₂). The spectra are normalised to the incident power. The excitation energy for each spectrum (2.33 eV for WS₂ and MoS₂, 1.96 eV for MoSe₂) is denoted as the green arrow. **(c)** Peak energy of upconversion photoluminescence in MoS₂ (open), MoSe₂ (solid), WS₂ (half left), and WSe₂ (half up) with the layer thickness ranging from 3L to 7L, and thicker than 7L.



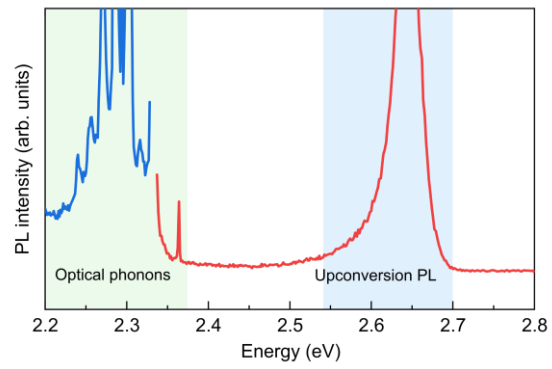
Extended Data Fig 1. Low-wavenumber Raman spectra of few-layer WSe₂ obtained with polarisation-resolved Raman spectroscopy. **a–b** Evolution of perpendicular mode (HV, including only shear mode) (**a**) and parallel mode (HH, including shear and breathing modes) (**b**) with layer thickness from 2L to 11L. In (**a**), the black dash line guides to the eyes. **c** Extracted frequencies of shear modes (S₁, S₂, S₃) as a function of the layer thickness.



Extended Data Fig 2. Photoluminescence spectrum of a 5L WSe₂ on a SiO₂/Si substrate obtained at $T = 80$ K.



Extended Data Fig 3. Power-dependent characteristics of light upconversion in layered WSe₂ at $T = 80$ K and excitation energy of 2.33 eV (wavelength 532 nm). **a,b** Evolution of upconversion photoluminescence in 5L **(a)** bulk WSe₂ **(b)** with power density from 0.03 to 1.02 mW/μm². Each spectrum is normalised by the power density. The black dashed lines are guides to the eyes. **c–h** Upconversion photoluminescence intensity as a function of incident power density P for 3L **(c)**, 4L **(d)**, 5L **(e)**, 6L **(f)**, 7L **(g)**, and 11L WSe₂ **(h)**. The black solid line in each figure represents a power-law exponent $\alpha = 2$.



Extended Data Fig 4. Optical phonons and photoluminescence spectrum of 5L WSe₂ at $T = 80$ K and excited with excitation energy of 2.33 eV.